Numerical analysis of Hahn echoes in solids

Pascal P. Man
Laboratoire de Chimie des Surfaces, CNRS URA 1428, Université Pierre et Marie Curie, 4 Place Jussieu, Tour 55, 75252 Paris Cedex 05, France
(Received 15 May 1995)

A numerical procedure for computing the Hahn echoes of half-integer quadrupole spins ($I=\frac{3}{2}$, $\frac{5}{2}$, $\frac{7}{2}$, and $\frac{9}{2}$) in solids has been derived from a detailed analysis of the evolution of the density operator. As the first-order quadrupole interaction is taken into account throughout the experiment, consisting in exciting the spin system with two in-phase pulses, the results are valid for any ratio of the quadrupole coupling, ω_Q, to the amplitude of the pulses, ω_{RF}. In the hard-pulse excitation condition ($\omega_Q/\omega_{RF} \ll 1$), the central-transition echo reaches the maximum when the first- and the second-pulse flip angles are equal to $\pi/2$ and π, respectively. On the other hand, all the echoes should be observed if the second-pulse flip angle is smaller than $\pi/2$; the optimum value of this angle depends on the spin I. The results on the central-transition echo in the soft-pulse excitation condition ($\omega_Q/\omega_{RF} \leq 50$), are presented. The two pulse flip angles should be optimized in order to observe the echo. Moreover, the study of the amplitude of the central-transition echo as a function of the second-pulse flip angle makes it possible to determine the value of ω_Q in a single crystal, or those of the quadrupole coupling constant and the asymmetry parameter in a powder.

I. INTRODUCTION

High-field superconducting magnets up to 11.7 T have dramatically simplified the investigation of half-integer quadrupole spins ($I=\frac{3}{2}$, $\frac{5}{2}$, $\frac{7}{2}$, and $\frac{9}{2}$) in solid-state NMR. The Periodic Table is formed to the extent of about 70% by this kind of nuclei, which are multiple-energy level systems, sensitive to the electric-field gradient (EFG) generated by their surroundings. Multiple-quantum transitions occurring in these systems make their study tedious, but, once understood, they provide valuable structural information.[1-3] Several data can be obtained: (i) Our first interest is the number of crystallographic sites available for an atom in a compound. If the popular magic angle spinning (MAS) of the sample at high speed cannot split the absorption lines, recent techniques such as double rotation[4] (DOR) and dynamic angle spinning[5] (DAS) provide a high-resolution spectrum in one and two dimensions, respectively. (ii) The true chemical shift of a line may be related to the mean bond angle.[6] As the quadrupole interaction also shifts the line, the determination of its contribution to the chemical shift requires the values of two quadrupole parameters: the quadrupole coupling constant $e^2qQ/\hbar$ and the asymmetry parameter η. Many techniques are available for this propose—line-shape analysis on the static or MAS spectrum,[7] analysis of usual spinning sidebands,[8] or those of the satellite transition spectroscopy[9] (SATRAS). (iii) The determination of the relative population of the different crystallographic sites in a compound remains a challenge. This kind of investigation requires the study of the radio-frequency (RF) excitation conditions of the spin system.[10,11] (iv) The presence of heteroatoms such as the proton, fluorine, or phosphorus in the vicinity of the studied atom can be detected by the cross-polarization method. Unfortunately, the line shape is distorted in an unpredictable way.[12] (v) The heteroatom distances can be determined using the Hahn spin-echo double resonance methods such as SEDOR, REDOR, or TEDOR.[13-15]

The Hahn spin-echo sequence[16] is mainly applied for refocusing magnetization lost in the dead time of the receiver[17] or distorted by spurious signals like ringing signals from the probe[18] when nuclei with low gyromagnetic ratios are studied. A permanent electric dipole in a single crystal such as $LiNbO_3$ also generates spurious signals that can be canceled by spin-echo sequences.[19] Sometimes, the spin-echo sequence is combined with the inversion-recovery sequence to measure the spin-lattice relaxation time T_1. The main difference between the Hahn spin-echo sequence and that of Solomon[20] is the following. In the first case, the interpulse delay is of the same order of magnitude as the duration T_{FID} of the free induction decay, whereas in the second case this delay must be smaller than T_{FID} (see Fig. 2) in order that the effect of magnetic-dipole interaction be neglected. As a result, there is no echo for the central transition in the Solomon spin-echo sequence; the echoes are satellite-transition signals. On the other hand, the echo for the central transition can be predicted in the Hahn spin-echo sequence if the heteronuclear magnetic-dipole interaction $H_{D(I-S)}$ is taken into account during the interpulse delay and the acquisition period.[21]

As integer spins are not numerous in the Periodic Table, we deal mainly with half-integer quadrupole spins. This paper presents a detailed analysis of Hahn echo formation and outlines a numerical procedure valid for the four half-integer quadrupole spins. The study of the Hahn echo amplitude versus the second-pulse flip angle allows us to determine the quadrupole parameters and, thus, the true chemical shift. The main advantage of spin-echo sequences over sample spinning techniques is the possibility of performing variable temperature experi-

ments. Our numerical procedure generates results identical with our former analytical results on spin $I=\frac{3}{2}$ (Refs. 21 and 22) and $\frac{5}{2}$ (Ref. 23) systems. Moreover, the RF excitation conditions for performing quantitative measurements also agree with our previous prediction.[24] We have to emphasize a limitation of our results: The homonuclear magnetic-dipole interaction $H_{D(I-I)}$, which is not taken into account in our analysis, must be much smaller than $H_{D(I-S)}$. The present study stems from the fact that if the analytical expressions for the spin $I=\frac{7}{2}$ system[25] can be obtained in a way similar to those for the spin $I=\frac{5}{2}$ system,[23,26] this is not the case for the spin $I=\frac{9}{2}$ system, which requires the solution of a fifth-degree equation. Until now, it has not been possible to solve it by radicals. This numerical procedure enables us to investigate spin $I=\frac{9}{2}$ systems without waiting for analytical results. In a further publication, we shall study the effects of $H_{D(I-S)}$ during the pulses on the Hahn echo amplitudes and compare our method with the SEDOR approach for the determination of the heteroatom distance.

II. THEORY

The energy levels of a half-integer quadrupole spin I in a strong static magnetic field B_0 are represented in Fig. 1. Two conventions are usually used to label these energy levels: (i) classically, using the magnetic number $|m\rangle$ and (ii) according to the fictitious spin-$\frac{1}{2}$ operator formalism $|I-m+1\rangle$.[27] In this paper, the first one is used. Second-order quadrupole effects, homonuclear magnetic-dipole interactions, as well as spin-relaxation phenomena, are assumed to be negligible. With these assumptions, the Hamiltonian (in angular frequency units) of the spin system, expressed in the rotating frame associated with the central transition, consists of three terms: a RF magnetic field $\omega_{RF}I_x$ along the $-x$ axis, a heteronuclear magnetic-dipole interaction $H_{D(I-S)}=\phi I_z$ with[28]

$$\phi=\frac{\mu_0\gamma_I\gamma_S\hbar S_z}{4\pi(r_{I-S})^3}[1-3\cos^2\theta_{I-S}]\ , \tag{1}$$

and the first-order quadrupole interaction,

$$H_Q^{(1)}=\frac{\omega_Q}{3}[3I_z^2-I(I+1)]\ , \tag{2a}$$

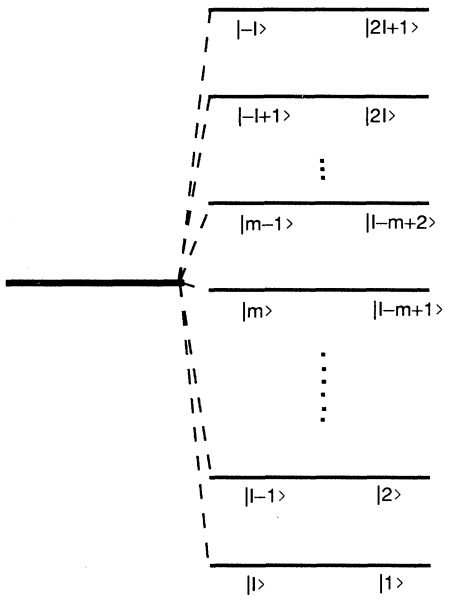

FIG. 1. The two conventions to label the energy levels of a quadrupole spin I in a strong static magnetic field.

with

$$\omega_Q=\frac{3e^2qQ}{8I(2I-1)\hbar}[3\cos^2\beta-1+\eta\sin^2\beta\cos2\alpha]\ . \tag{2b}$$

The Euler angles α and β orient B_0 in the principal axis system of the EFG tensor. Our quadrupole coupling ω_Q is equal to half the standard one,[29] which means that two consecutive absorption lines in the spectrum of a single crystal are separated by $2\omega_Q$. For polycrystalline samples, the quadrupole coupling constant $e^2qQ/\hbar$ and the asymmetry parameter η are the relevant quantities.

The Hahn echo sequence consisting of two $-x$ pulses is represented in Fig. 2. The main differences between the assumptions in the original Hahn echo sequence[16] and the present case are (i) the consideration of $H_Q^{(1)}$ throughout the experiment and (ii) in early work[30–34] the magnetic interaction ϕI_z represented the inhomogeneity of B_0, and in our case, this term corresponds to $H_{D(I-S)}$.

The spin dynamics during the detection period τ_4 can be described by the density operator

$$\rho(t_1,\tau_2,t_3,\tau_4)=\exp(-iH^{(c)}\tau_4)\exp(-iH^{(a)}t_3)\exp(-iH^{(c)}\tau_2)\exp(-iH^{(a)}t_1)$$
$$\times\rho(0)\exp(iH^{(a)}t_1)\exp(iH^{(c)}\tau_2)\exp(iH^{(a)}t_3)\exp(iH^{(c)}\tau_4) \tag{3}$$

with

$$H^{(a)}=\omega_{RF}I_x+H_Q^{(1)}\ ,\quad H^{(c)}=H_Q^{(1)}+\phi I_z\ ,\quad \rho(0)=I_z\ . \tag{4}$$

Throughout the paper, the matrices associated with Hamiltonians and density operators are expressed in the eigenstates $|m\rangle$ of I_z. Using the diagonalized form Ω of $H^{(a)}$ and the transformation operator T related by

$$\Omega=T^+H^{(a)}T\ , \tag{5}$$

Eq. (3) becomes

$$\rho(t_1,\tau_2,t_3,\tau_4)=\exp(-iH^{(c)}\tau_4)T\exp(-i\Omega t_3)T^+\exp(-iH^{(c)}\tau_2)T\exp(-i\Omega t_1)$$
$$\times T^+\rho(0)T\exp(i\Omega t_1)T^+\exp(iH^{(c)}\tau_2)T\exp(i\Omega t_3)T^+\exp(iH^{(c)}\tau_4)\ . \tag{6}$$

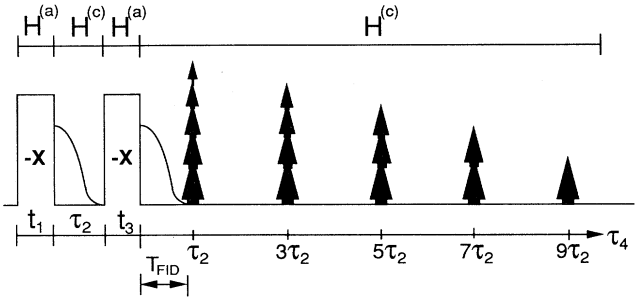

FIG. 2. Hamiltonians, pulse sequence and the Hahn echoes for a spin $I=\frac{9}{2}$ system, depicted schematically by arrows whose heights and widths are meaningless. In fact, mainly the $\tau_4=\tau_2$ echoes are observed experimentally. The other echoes, if observed, should be located at odd numbers of the interpulse delay τ_2. The broadest arrows represent the echoes of the central transition, whereas the thinnest arrow represents the echoes of the outermost satellite transitions.

A simple-minded approach consists of calculating the density operator at $\tau_4=\tau_2$ to predict the Hahn echoes. As the spin-relaxation phenomena have not been taken into account, the numerical computation of the density operator in the detection period τ_4 [Eq. (6)] yields the contribution of the FID following the second pulse as well as that of the echoes. In order to separate these two contributions, we analyze the evolution of the density operator from the initial state $\rho(0)$ to the detection period in some detail. Then we derive a numerical procedure, which is valid for the four half-integer quadrupole spins, to compute only the contribution of the echoes.

The density operator $\rho(t_1)$ at the end of the first $-x$ pulse is given by

$$\rho(t_1)=T\exp(-i\Omega t_1)T^{+}\rho(0)T\exp(i\Omega t_1)T^{+} . \quad (7)$$

In fact, a matrix element $\rho_{p,q}(t_1)$ of $\rho(t_1)$, located *above* the principal diagonal of the matrix of $\rho(t_1)$, represents the "line intensity" $\langle I_{-}^{p,q}(t_1)\rangle$ of the corresponding transition ($p\leftrightarrow q$), that is,

$$\rho_{p,q}(t_1)\equiv\langle I_{-}^{p,q}(t_1)\rangle=\mathrm{Tr}[\rho(t_1)I_x^{p,q}] -i\,\mathrm{Tr}[\rho(t_1)I_y^{p,q}] , \quad (8)$$

Tr denotes a trace. The subscripts p and q are magnetic numbers satisfying $p>q$. They locate the matrix element $\rho_{p,q}(t_1)$ at the $(I-p+1)$th row and the $(I-q+1)$th column of the associated matrix. The matrices of the operators $I_x^{p,q}$ and $I_y^{p,q}$ in the eigenstates of I_z have the following form:[28]

$$I_x^{p,q}=\begin{array}{c} \\ \langle I| \\ \langle p| \\ \langle p-1| \\ \\ \langle q| \\ \langle -I| \end{array}\begin{array}{c} \begin{array}{cccccc} |I\rangle & |p\rangle & |p-1\rangle & & |q\rangle & |-I\rangle \end{array} \\ \begin{bmatrix} & & & & & \\ & & & & 1/2 & \\ & & & & & \\ & & & & & \\ & 1/2 & & & & \\ & & & & & \end{bmatrix} \end{array} , \quad (9a)$$

$$I_y^{p,q}=\begin{array}{c} \\ \langle I| \\ \langle p| \\ \langle p-1| \\ \\ \langle q| \\ \langle -I| \end{array}\begin{array}{c} \begin{array}{cccccc} |I\rangle & |p\rangle & |p-1\rangle & & |q\rangle & |-I\rangle \end{array} \\ \begin{bmatrix} & & & & & \\ & & & & -i/2 & \\ & & & & & \\ & & & & & \\ & i/2 & & & & \\ & & & & & \end{bmatrix} \end{array} . \quad (9b)$$

These two matrices have only two nonzero elements. For completeness, a matrix element located *below* the principal diagonal is defined by

$$\rho_{a,b}(t_1)\equiv\langle I_{+}^{b,a}(t_1)\rangle =\mathrm{Tr}[\rho(t_1)I_x^{b,a}]+i\,\mathrm{Tr}[\rho(t_1)I_y^{b,a}] . \quad (10)$$

The subscripts a and b are magnetic numbers satisfying $a<b$.

After the first pulse, the evolution of the spin system is described by

$$\rho(t_1,\tau_2)=\exp(-iH^{(c)}\tau_2)\rho(t_1)\exp(iH^{(c)}\tau_2) , \quad (11)$$

and the effect of the second pulse by

$$\rho(t_1,\tau_2,t_3)=T\exp(-i\Omega t_3)T^{+}\rho(t_1,\tau_2) \times T\exp(i\Omega t_3)T^{+} . \quad (12)$$

During the detection period, the density operator becomes

$$\rho(t_1,\tau_2,t_3,\tau_4)=\exp(-iH^{(c)}\tau_4)\rho(t_1,\tau_2,t_3) \times\exp(iH^{(c)}\tau_4) . \quad (13)$$

Only the matrix elements of $\rho(t_1,\tau_2,t_3,\tau_4)$ associated with single quantum ($m-1\leftrightarrow m$) transitions are required because they are observable experimentally, namely,

$$\rho_{m-1,m}(t_1,\tau_2,t_3,\tau_4)=\exp(-i\tau_4\{\tfrac{1}{3}\omega_Q[3(m-1)^2-I(I+1)]+[m-1]\phi\}) \times\rho_{m-1,m}(t_1,\tau_2,t_3)\exp(i\tau_4\{\tfrac{1}{3}\omega_Q[3m^2-I(I+1)]+m\phi\}) =\rho_{m-1,m}(t_1,\tau_2,t_3)\exp\{i\tau_4[(2m-1)\omega_Q+\phi]\} . \quad (14)$$

m is a magnetic number. The matrix elements $\rho_{m-1,m}(t_1,\tau_2,t_3)$ are those of the density operator $\rho(t_1,\tau_2,t_3)$ at the end of the second pulse. The subscripts $(m-1,m)$ in Eq. (14) locate the matrix element at the $(I-m+1)$th row and the

$(I-m+2)$th column of the associated matrix, that is, in the first diagonal line *below* the principal diagonal.

Our aim is to analyze the Hahn echo amplitudes. Once the matrix elements $\rho^E_{m-1,m}(t_1,\tau_2,t_3,\tau_4)$ of the echo density operator are determined, the *relative* echo amplitudes for the x and y components of the $(m-1\leftrightarrow m)$ transitions are defined by

$$E_x^{m-1,m}(t_1,\tau_2,t_3,\tau_4)+iE_y^{m-1,m}(t_1,\tau_2,t_3,\tau_4)=\frac{\sqrt{I(I+1)-m(m-1)}}{\frac{1}{3}I(I+1)(2I+1)}\rho^E_{m-1,m}(t_1,\tau_2,t_3,\tau_4)\ . \tag{15}$$

From Eq. (14), we deduce that only a part of each matrix element $\rho_{m-1,m}(t_1,\tau_2,t_3)$ in Eq. (12) containing terms such as $\exp\{-ni\tau_2[(2m-1)\omega_Q+\phi]\}$ is relevant for the analysis of the echoes, where n is a positive integer. This also means that only the matrix elements $\rho_{m-1,m}(t_1,\tau_2)$ of the density operator $\rho(t_1,\tau_2)$ containing the same exponential functions are involved. All of them are located *above* the principal diagonal of the corresponding matrix. As a result, we can consider a simplified density operator $\rho^S(t_1,\tau_2)$ whose matrix elements are given by

$$\begin{aligned}\rho^S_{r,c}(t_1,\tau_2)&=\exp(-i\tau_2\{\tfrac{1}{3}\omega_Q[3r^2-I(I+1)]+r\phi\})\rho_{r,c}(t_1)\exp(i\tau_2\{\tfrac{1}{3}\omega_Q[3c^2-I(I+1)]+c\phi\})\\&=\rho_{r,c}(t_1)\exp\{-i\tau_2[r-c][(r+c)\omega_Q+\phi]\}\ .\end{aligned} \tag{16}$$

The two conditions on the values of r and c are $r+c=2m-1$ and $r>c$. The latter condition is obvious because the matrix elements $\rho^S_{r,c}(t_1,\tau_2)$ are located *above* the principal diagonal of the corresponding matrix. Consider the biggest spin, which is $I=\frac{9}{2}$. For the central-transition echoes, that is, $m=\frac{1}{2}$, the values for r and c are $(r,-r)=(\frac{9}{2},-\frac{9}{2})$, $(\frac{7}{2},-\frac{7}{2})$, $(\frac{5}{2},-\frac{5}{2})$, $(\frac{3}{2},-\frac{3}{2})$, and $(\frac{1}{2},-\frac{1}{2})$; five matrix elements are involved. For the satellite-transition echoes, these parameters and the matrix elements involved are given in Table I. These values of (r,c) also concern with the density operator $\rho(t_1)$ in Eq. (16). They generate a simplified density operator $\rho^S(t_1)$, the nonzero matrix elements of which are located *above* the principal diagonal.

Proceed one step further by including the exponential functions contained in Eq. (14) in the matrix of $\rho^S(t_1,\tau_2)$. This transformation leads to a new simplified density operator $\rho^S(t_1,\tau_2,\tau_4)$ whose matrix is reported in Table II. This table represents the matrix for a spin $I=\frac{9}{2}$ system. Deleting the two outermost rows and the two outermost columns generates the 8×8 matrix for $I=\frac{7}{2}$. The rectangle in Table II encloses the matrix elements for $I=\frac{5}{2}$.

The effect of the second pulse on $\rho^S(t_1,\tau_2,\tau_4)$ is described by

$$\begin{aligned}\rho^E(t_1,\tau_2,t_3,\tau_4)=&T\exp(-i\Omega t_3)T^+\rho^S(t_1,\tau_2,\tau_4)\\&\times T\exp(i\Omega t_3)T^+\ .\end{aligned} \tag{17}$$

Equations (7) and (17) have a similar form. In the first case, the initial state is described by $\rho(0)$, whereas in the second it is given by $\rho^S(t_1,\tau_2,\tau_4)$. The first pulse converts the thermal equilibrium magnetization I_z into "line intensities" $\langle I^{p,q}_-(t_1)\rangle$, $\langle I^{b,a}_+(t_1)\rangle$, and other magnetizations. The second pulse refocuses as echoes the line intensities $\langle I^{r,c}_-(t_1)\rangle$ (Table II) generated by the first pulse. To reiterate, the study of the Hahn echoes requires the determination of only $2I$ matrix elements $\rho^E_{m-1,m}(t_1,\tau_2,t_3,\tau_4)$ of Eq. (17) located in the first diagonal line *below* the

TABLE I. Matrix elements $\rho^S_{r,c}$ of the simplified density operators $\rho^S(t_1,\tau_2,\tau_4)$, $\rho^S(t_1,\tau_2)$, and $\rho^S(t_1)$ involved in the echo formation.

Transitions $m-1\leftrightarrow m$	m	r,c	$I=9/2$	$I=7/2$	$I=5/2$	$I=3/2$	
$7/2\leftrightarrow9/2$	$9/2$	$r,-r+8$	$9/2,7/2$				
$5/2\leftrightarrow7/2$	$7/2$	$r,-r+6$	$9/2,3/2$	$7/2,5/2$			
$3/2\leftrightarrow5/2$	$5/2$	$r,-r+4$	$9/2,-1/2$	$7/2,1/2$	$5/2,3/2$		
$1/2\leftrightarrow3/2$	$3/2$	$r,-r+2$	$9/2,-5/2$	$7/2,-3/2$	$5/2,-1/2$	$3/2,1/2$	
$-1/2\leftrightarrow1/2$	$1/2$	$r,-r$	$9/2,-9/2$	$7/2,-7/2$	$5/2,-5/2$	$3/2,-3/2$	$1/2,-1/2$
$-3/2\leftrightarrow-1/2$	$-1/2$	$r,-r-2$	$5/2,-9/2$	$3/2,-7/2$	$1/2,-5/2$	$-1/2,-3/2$	
$-5/2\leftrightarrow-3/2$	$-3/2$	$r,-r-4$	$1/2,-9/2$	$-1/2,-7/2$	$-3/2,-5/2$		
$-7/2\leftrightarrow-5/2$	$-5/2$	$r,-r-6$	$-3/2,-9/2$	$-5/2,-7/2$			
$-9/2\leftrightarrow-7/2$	$-7/2$	$r,-r-8$	$-7/2,-9/2$				

TABLE II. Simplified density matrix $\rho^S(t_1,\tau_2,\tau_4)$. For clarity, $\langle I_-^{9/2,7/2}\rangle_{\tau_2}(8\omega_Q+\phi)$ means $\langle I_-^{9/2,7/2}(t_1)\rangle\exp[i(\tau_4-\tau_2)(8\omega_Q+\phi)]$.

	$\lvert 9/2\rangle$	$\lvert 7/2\rangle$	$\lvert 5/2\rangle$	$\lvert 3/2\rangle$	$\lvert 1/2\rangle$	$\lvert -1/2\rangle$	$\lvert -3/2\rangle$	$\lvert -5/2\rangle$	$\lvert -7/2\rangle$	$\lvert -9/2\rangle$
		$\langle I_-^{9/2,7/2}\rangle$		$\langle I_-^{9/2,3/2}\rangle$		$\langle I_-^{9/2,-1/2}\rangle$		$\langle I_-^{9/2,-5/2}\rangle$		$-i\langle I_y^{9/2,-9/2}\rangle$
$\langle 9/2\rvert$	0		0		0		0		0	
		$\tau_2(8\omega_Q+\phi)$		$3\tau_2(6\omega_Q+\phi)$		$5\tau_2(4\omega_Q+\phi)$		$7\tau_2(2\omega_Q+\phi)$		$9\tau_2\phi$
			$\langle I_-^{7/2,5/2}\rangle$		$\langle I_-^{7/2,1/2}\rangle$		$\langle I_-^{7/2,-3/2}\rangle$		$-i\langle I_y^{7/2,-7/2}\rangle$	
$\langle 7/2\rvert$	0	0		0		0		0		0
			$\tau_2(6\omega_Q+\phi)$		$3\tau_2(4\omega_Q+\phi)$		$5\tau_2(2\omega_Q+\phi)$		$7\tau_2\phi$	
				$\langle I_-^{5/2,3/2}\rangle$		$\langle I_-^{5/2,-1/2}\rangle$		$-i\langle I_y^{5/2,-5/2}\rangle$		$\langle I_-^{5/2,-9/2}\rangle$
$\langle 5/2\rvert$	0	0	0		0		0		0	
				$\tau_2(4\omega_Q+\phi)$		$3\tau_2(2\omega_Q+\phi)$		$5\tau_2\phi$		$7\tau_2(-2\omega_Q+\phi)$
					$\langle I_-^{3/2,1/2}\rangle$		$-i\langle I_y^{3/2,-3/2}\rangle$		$\langle I_-^{3/2,-7/2}\rangle$	
$\langle 3/2\rvert$	0	0	0	0		0		0		0
					$\tau_2(2\omega_Q+\phi)$		$3\tau_2\phi$		$5\tau_2(-2\omega_Q+\phi)$	
						$-i\langle I_y^{1/2,-1/2}\rangle$		$\langle I_-^{1/2,-5/2}\rangle$		$\langle I_-^{1/2,-9/2}\rangle$
$\langle 1/2\rvert$	0	0	0	0	0		0		0	
						$\tau_2\phi$		$3\tau_2(-2\omega_Q+\phi)$		$5\tau_2(-4\omega_Q+\phi)$
							$\langle I_-^{-1/2,-3/2}\rangle$		$\langle I_-^{-1/2,-7/2}\rangle$	
$\langle -1/2\rvert$	0	0	0	0	0	0		0		0
							$\tau_2(-2\omega_Q+\phi)$		$3\tau_2(-4\omega_Q+\phi)$	
								$\langle I_-^{-3/2,-5/2}\rangle$		$\langle I_-^{-3/2,-9/2}\rangle$
$\langle -3/2\rvert$	0	0	0	0	0	0	0		0	
								$\tau_2(-4\omega_Q+\phi)$		$3\tau_2(-6\omega_Q+\phi)$
									$\langle I_-^{-5/2,-7/2}\rangle$	
$\langle -5/2\rvert$	0	0	0	0	0	0	0	0		0
									$\tau_2(-6\omega_Q+\phi)$	
										$\langle I_-^{-7/2,-9/2}\rangle$
$\langle -7/2\rvert$	0	0	0	0	0	0	0	0	0	
										$\tau_2(-8\omega_Q+\phi)$
$\langle -9/2\rvert$	0	0	0	0	0	0	0	0	0	0

principal diagonal of the matrix associated with $\rho^E(t_1,\tau_2,t_3,\tau_4)$.

It is worth noting that each matrix element of $\rho^S(t_1,\tau_2,\tau_4)$ is associated with one particular Hahn echo, the nature (central-transition echo or satellite-transition echo) and the location (in the detection period τ_4) of which are already indicated in this matrix, explicitly for its location but implicitly for its nature. For a spin I system smaller than $\frac{9}{2}$, as already mentioned above, only a part of this matrix is useful. For example, if $I=\frac{5}{2}$, the echo of the $(\frac{3}{2}\leftrightarrow\frac{5}{2})$ satellite transition represents the refocusing of the line intensity $\langle I_-^{5/2,3/2}(t_1)\rangle$ involved in

$$\rho^S_{5/2,3/2}(t_1,\tau_2,\tau_4)=\langle I_-^{5/2,3/2}(t_1)\rangle \times\exp[i(\tau_4-\tau_2)(4\omega_Q+\phi)]\ , \quad (18)$$

which shows that the echo is located at $\tau_4=\tau_2$. Similarly, the two echoes of the $(\frac{1}{2}\leftrightarrow\frac{3}{2})$ satellite transition originate from the two matrix elements,

$$\rho^S_{3/2,1/2}(t_1,\tau_2,\tau_4)=\langle I_-^{3/2,1/2}(t_1)\rangle \times\exp[i(\tau_4-\tau_2)(2\omega_Q+\phi)]\ , \quad (19a)$$

$$\rho^S_{5/2,-1/2}(t_1,\tau_2,\tau_4)=\langle I_-^{5/2,-1/2}(t_1)\rangle \times\exp[i(\tau_4-3\tau_2)(2\omega_Q+\phi)]\ , \quad (19b)$$

respectively. They occur at $\tau_4=\tau_2$ and $\tau_4=3\tau_2$ and represent the refocusing of $\langle I_-^{3/2,1/2}(t_1)\rangle$ and $\langle I_-^{5/2,-1/2}(t_1)\rangle$, respectively. The three matrix elements,

$$\rho^S_{1/2,-1/2}(t_1,\tau_2,\tau_4)=-i\langle I_y^{1/2,-1/2}(t_1)\rangle \times\exp[i(\tau_4-\tau_2)\phi]\ , \quad (20a)$$

$$\rho^S_{3/2,-3/2}(t_1,\tau_2,\tau_4)=-i\langle I_y^{3/2,-3/2}(t_1)\rangle \times\exp[i(\tau_4-3\tau_2)\phi]\ , \quad (20b)$$

$$\rho^S_{5/2,-5/2}(t_1,\tau_2,\tau_4)=-i\langle I_y^{5/2,-5/2}(t_1)\rangle \times\exp[i(\tau_4-5\tau_2)\phi]\ , \quad (20c)$$

are associated with the three echoes of the central transition $(-\frac{1}{2}\leftrightarrow\frac{1}{2})$. These echoes are located at $\tau_4=\tau_2$, $\tau_4=3\tau_2$, and $\tau_4=5\tau_2$ and correspond to the refocusing of $\langle I_y^{1/2,-1/2}(t_1)\rangle$, $\langle I_y^{3/2,-3/2}(t_1)\rangle$, and $\langle I_y^{5/2,-5/2}(t_1)\rangle$, respectively. The two matrix elements $\rho^S_{-1/2,-3/2}(t_1,\tau_2,\tau_4)$ and $\rho^S_{1/2,-5/2}(t_1,\tau_2,\tau_4)$ describe the two echoes of the $(-\frac{3}{2}\leftrightarrow-\frac{1}{2})$ satellite transition, and $\rho^S_{-3/2,-5/2}(t_1,\tau_2,\tau_4)$ characterizes the echo of the $(-\frac{5}{2}\leftrightarrow-\frac{3}{2})$ satellite transition. From a theoretical point of view, for the $(m-1\leftrightarrow m)$ transition, $N(=I+\frac{1}{2}-|m-\frac{1}{2}|)$ echoes located at $\tau_4=(r-c)\tau_2$ should be observed. The quantum numbers r, c, and m are related by $r+c=2m-1$ and $r>c$, as already mentioned above.

III. NUMERICAL PROCEDURE AND RESULTS

From now, we focus on the maximum value $E_y^{m-1,m}(t_1,\tau_2,t_3,\tau_4=(r-c)\tau_2)$ of the relative echo amplitude, which is proportional to the area of the associated absorption line. Knowledge of the echo positions, $\tau_4=(r-c)\tau_2$, allows us to compute $E_y^{m-1,m}(t_1,\tau_2,t_3,\tau_4=(r-c)\tau_2)$ using $\rho^S(t_1)\equiv\rho^S(t_1,\tau_2=\tau_4=0)$ instead of $\rho^S(t_1,\tau_2,\tau_4)$. As a result, Eq. (17) reduces to

$$\rho^E(t_1,t_3)=T\exp(-i\Omega t_3)T^+\rho^S(t_1)T\exp(i\Omega t_3)T^+\ . \quad (21)$$

Equations (17) and (21) and the way of writing $\rho^S(t_1,\tau_2,\tau_4)$ (see Table II) are the key points of our numerical procedure. Once the two matrices Ω and T [see Eq. (5)] are computed by a numerical matrix diagonalization method, the matrix of $\rho(t_1)$ is obtained using Eq. (7). Then, the matrix multiplications in Eq. (21) are carried out with $\rho^S(t_1)$ containing a *single* nonzero term $\langle I_-^{r,c}(t_1)\rangle$ extracted from $\rho(t_1)$. Finally, the value of $E_y^{m-1,m}(t_1,\tau_2,t_3,\tau_4=(r-c)\tau_2)$ can be obtained by taking the imaginary part of $\rho^E_{m-1,m}(t_1,t_3)$, times a constant term, as in Eq. (15). We represent these results by

$$E_y^{m-1,m}(t_1,\tau_2,t_3,\tau_4=(r-c)\tau_2)=\frac{\sqrt{I(I+1)-m(m-1)}}{\frac{1}{3}I(I+1)(2I+1)}\langle I_y^{r,c}(t_1)\rangle\Psi^{m,m-1}(t_3,\tau_4=(r-c)\tau_2)\ . \quad (22)$$

Therefore, $E_y^{m-1,m}(t_1,\tau_2,t_3,\tau_4=(r-c)\tau_2)$ is the product of two quantities: The first one is the imaginary part $\langle I_y^{r,c}(t_1)\rangle$ of the single nonzero matrix element of $\rho^S(t_1)$, which depends on the first-pulse duration t_1; the second quantity, $\Psi^{m,m-1}(t_3,\tau_4=(r-c)\tau_2)$, generated by Eq. (21), depends on the second-pulse duration t_3.

To our knowledge, mainly the $\tau_4=\tau_2$ echoes are observed experimentally. The $\tau_4=3\tau_2$ echoes in a spin $I=\frac{3}{2}$ system have been detected in a ferromagnetic material and explained by Abelyashev *et al.*[35] From a practical point of view, we restrict ourselves to the study of the $\tau_4=\tau_2$ echoes, postponing the investigation of the other echoes until experimental results are available. This means that the $(m-1\leftrightarrow m)$ transition echo is the refocusing, by the second pulse, of the single-quantum line intensity $\langle I_-^{m,m-1}(t_1)\rangle$ located in the first diagonal line *above* the principal diagonal of $\rho^S(t_1)$. The $2I$ maximum echo amplitudes,

$$E_y^{m-1,m}(t_1,\tau_2,t_3,\tau_4=\tau_2)=\frac{\sqrt{I(I+1)-m(m-1)}}{\frac{1}{3}I(I+1)(2I+1)}\langle I_y^{m,m-1}(t_1)\rangle\Psi^{m,m-1}(t_3,\tau_4=\tau_2)\ , \quad (23)$$

must be computed *independently*. Then, adding the result together yields the total amplitude of all the $\tau_4=\tau_2$ echoes. In other words, for the spin $I=\frac{9}{2}$ system, we have to apply Eq. (7) once and Eq. (21) nine times.

Figure 3 represents the functions $E_y^{m-1,m}(t_1,\tau_2,t_3,\tau_4=\tau_2)$ for the four half-integer quadrupole spins $I=\frac{3}{2}$, $\frac{5}{2}$, $\frac{7}{2}$, and $\frac{9}{2}$ versus the second-pulse flip angle $\omega_{RF}t_3$. The first-pulse flip angle is $\omega_{RF}t_1=\pi/2$. The excitation of the spin system is supposed to be nonselective ($\omega_Q/\omega_{RF}\ll 1$),[11] and it is also called the *hard*-pulse excitation condition. From a theoretical point of view, the effect to the first-order quadrupole interaction can be neglected during the pulses. The spin dynamics during the pulses can be described simply with the Wigner rotation matrices.[33,34] The graphs of the total $\tau_4=\tau_2$ Hahn echo amplitudes for these four spins are shown in Fig. 4. The amplitude of the central-transition echo reaches a maximum if the first- and the second-pulse flip angles are equal to $\pi/2$ and π, respectively. This is the well-known $t_{90°}$-τ-$t_{180°}$-2τ pulse sequence,[16] $t_{90°}$ being the pulse duration defined by $\omega_{RF}t_{90°}=\pi/2$. On the other hand, the detection of all the $\tau_4=\tau_2$ Hahn echoes requires a second-pulse flip angle smaller than $\pi/2$, corresponding to the first maximum of the graphs in Fig. 4. The graphs in Figs. 3 and 4 are exactly those reported by Mehring and Kanert.[33,34] These results prove the correctness of our numerical procedure. These graphs are characteristic of a small ω_Q/ω_{RF} ratio. For example, consider the case of $I=\frac{5}{2}$: The maximum echo amplitude of the central transition goes through three maxima for $0\le\omega_{RF}t_3\le\pi$, those of the $(\frac{1}{2}\leftrightarrow\frac{3}{2})$ and $(-\frac{3}{2}\leftrightarrow-\frac{1}{2})$ satellite transitions have two maxima, whereas those of the $(\frac{3}{2}\leftrightarrow\frac{5}{2})$ and $(-\frac{5}{2}\leftrightarrow-\frac{3}{2})$ satellite transitions have only one maximum. As a result, the study of the $\tau_4=\tau_2$ Hahn echo amplitudes versus the second-pulse flip angle allows us to detect the presence of a small quadrupole coupling ω_Q generated by defects in a crystal.[33,34] In contrast, the study of the central-line intensity obtained with a one-pulse sequence versus the pulse flip angle (see Fig. 5) is inefficient for detecting the presence of a small quadrupole coupling if the absorption lines are not resolved.

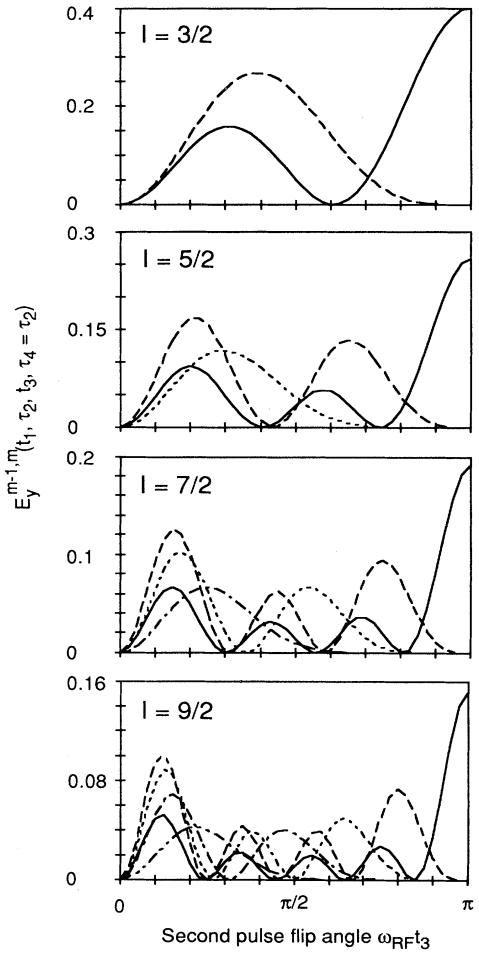

FIG. 3. Graphs of the $\tau_4=\tau_2$ Hahn echo amplitudes in the hard-pulse excitation condition ($\omega_Q/\omega_{RF}\ll 1$) vs the second-pulse flip angle $\omega_{RF}t_3$. (——): $(-\frac{1}{2}\leftrightarrow\frac{1}{2})$ echo; (— — —): $(\frac{1}{2}\leftrightarrow\frac{3}{2})$ and $(-\frac{3}{2}\leftrightarrow-\frac{1}{2})$ echoes; (. . . .): $(\frac{3}{2}\leftrightarrow\frac{5}{2})$ and $(-\frac{5}{2}\leftrightarrow-\frac{3}{2})$ echoes; (—·—·—·): $(\frac{5}{2}\leftrightarrow\frac{7}{2})$ and $(-\frac{7}{2}\leftrightarrow-\frac{5}{2})$ echoes; and (—··—··—··): $(\frac{7}{2}\leftrightarrow\frac{9}{2})$ and $(-\frac{9}{2}\leftrightarrow-\frac{7}{2})$ echoes. The first-pulse flip angle $\omega_{RF}t_1$ is $\pi/2$.

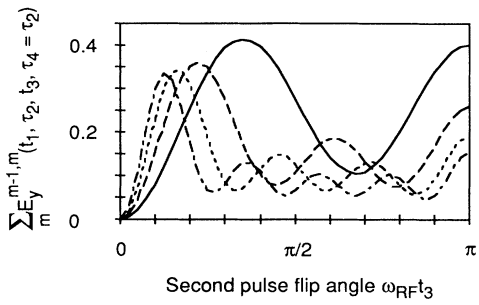

FIG. 4. Graphs of the total $\tau_4=\tau_2$ Hahn echo amplitudes of Fig. 3 vs the second-pulse flip angle $\omega_{RF}t_3$. (——): $I=\frac{3}{2}$; (— — —): $I=\frac{5}{2}$; (. . . .): $I=\frac{7}{2}$; and (—·—·—·): $I=\frac{9}{2}$.

As the hard-pulse excitation condition is not always fulfilled, we extend the investigation to the *soft*-pulse case, that is, the ω_Q/ω_{RF} ratio can take any value ranging from 0 to 50 or more. Now we deal with the $\tau_4=\tau_2$ echo of the central transition acquired with two soft pulses. From a theoretical point of view, the first-order quadrupole interaction must be taken into account during the two pulses. Therefore, this interaction is present throughout the experiment, as shown in Fig. 2. We do not study the echo amplitudes of the satellite transitions, which decrease towards zero when the ω_Q/ω_{RF} ratio increases; furthermore, they are not always observed in a powdered sample. As mentioned above, see Eq. (22), $E_y^{-1/2,1/2}(t_1,\tau_2,t_3,\tau_4=\tau_2)$ is the product of two functions, which can be analyzed separately.

Figure 5 represents the function $\langle I_y^{1/2,-1/2}(t_1)\rangle$, which is related to the central-line intensity generated by the first pulse, versus the first-pulse flip angle $\omega_{RF}t_1$, for the four half-integer quadrupole spins and for several ω_Q/ω_{RF} ratios. The well-known results are that the first

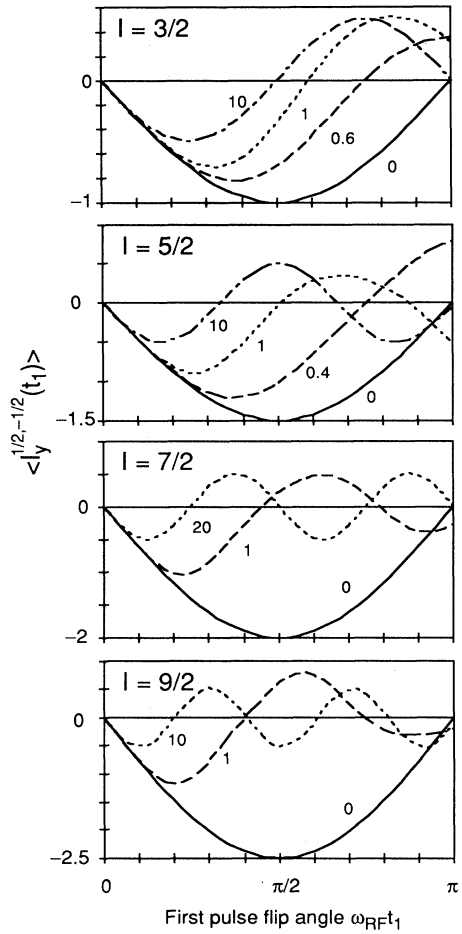

FIG. 5. Graphs of the line intensity $\langle I_y^{1/2,-1/2}(t_1)\rangle$ vs the first-pulse flip angle $\omega_{RF}t_1$, for $I=\frac{3}{2}$, $\frac{5}{2}$, $\frac{7}{2}$, and $\frac{9}{2}$. The numbers correspond to ω_Q/ω_{RF} ratios.

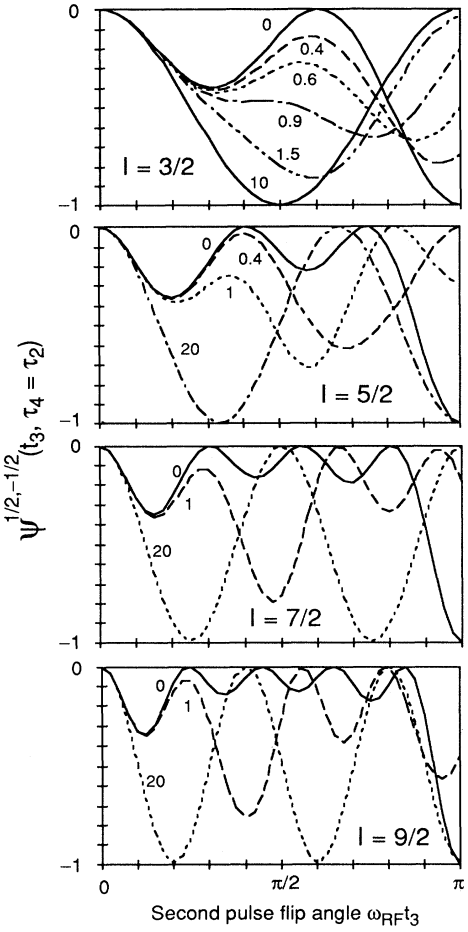

FIG. 6. Graphs of the function $\Psi^{1/2,-1/2}(t_3,\tau_4=\tau_2)$ vs the second-pulse flip angle $\omega_{RF}t_3$, for $I=\frac{3}{2}$, $\frac{5}{2}$, $\frac{7}{2}$, and $\frac{9}{2}$. The numbers correspond to ω_Q/ω_{RF} ratios.

maximum of the line intensity and the associated pulse flip angle decrease when the ω_Q/ω_{RF} ratio increases, but both reach limiting values that are $1/(I+\frac{1}{2})$ of those obtained with the hard-pulse excitation condition. The dependence of these line intensities on the pulse flip angle is more or less sinusoidal. When the pulse flip angle is small, the line intensity $\langle I_y^{1/2,-1/2}(t_1)\rangle$ depends linearly on this angle but becomes independent of the ω_Q/ω_{RF} ratio. Therefore, with a powdered sample, which presents a distribution of ω_Q, a small pulse flip angle must be applied in order to get rid of the effect of the first-order quadrupole interaction on the line intensity.

Figure 6 represents the functions $\Psi^{1/2,-1/2}(t_3,\tau_4=\tau_2)$ versus the second-pulse flip angle $\omega_{RF}t_3$, for the four half-integer quadrupole spins and for several ω_Q/ω_{RF} ratios. The graphs of the spins $I=\frac{3}{2}$ and $\frac{5}{2}$ are exactly those obtained previously by us using analytical expressions.[21–23] These two numerical results support, once more, the validity of our procedure. The graphs of the spins $I=\frac{7}{2}$ and $\frac{9}{2}$ are new results. All of the functions $\Psi^{1/2,-1/2}(t_3,\tau_4=\tau_2)$ are negative. In fact, alternating the phase of the second pulse does not change the sign of these functions.[21,22] Two facts have to be noted: (i) The dependence of $\Psi^{1/2,-1/2}(t_3,\tau_4=\tau_2)$ on the second-pulse flip angle presents more extrema than does the function $\langle I_y^{1/2,-1/2}(t_1)\rangle$ except for high ω_Q/ω_{RF} ratios; see Fig. 4. (ii) When the second-pulse flip angle is small, this function also becomes independent of the ω_Q/ω_{RF} ratio. In fact, it depends on the pulse flip angle quadratically.[24] When the ω_Q/ω_{RF} ratio is larger than 10, mainly the echo of the central transition is detected. Figures 5 and 6 show that the echo amplitude is at a peak if the first- and the second-pulse flip angles are equal to $t_{90°}/(I+\frac{1}{2})$ and $2t_{90°}/(I+\frac{1}{2})$, respectively. These excitation conditions are the quadrupole generalization of the Hahn echo sequence applied to the central transition, valid for a strong ω_Q/ω_{RF} ratio.[24,36] With a powdered sample, to get rid of the effect of the first-order quadrupole interaction on the central-transition echo amplitude, the two pulse flip angles must be small. Moreover, as the interpulse delay τ_2 is in the same order of magnitude as the duration T_{FID}, the spin-echo relaxation time T_{2E} must be determined in

order to correct the experimental echo amplitude for quantitative results.

So far, the numerical procedure has concerned single crystals where the important parameter is the quadrupole coupling ω_Q. In practice, the sample is in powder form. As a result, to apply this procedure, the powder pattern of ω_Q, which depends on the quadrupole coupling constant and the asymmetry parameter, has to be used.[37]

IV. CONCLUSIONS

A numerical procedure for the Hahn echoes of half-integer quadrupole spins in solids has been derived from a detailed analysis of the evolution of the density operator. The presence of the heteronuclear magnetic-dipole interaction ϕI_z between the two pulses and in the detection period is required to predict the echoes for the central transition. As this interaction has been neglected during the pulses, its effect on the echo amplitudes has not been predicted. However, there is no difficulty in taking into account this interaction throughout the experiment in the numerical procedure. In this case, the analysis of the Hahn echo amplitude as a function of the second-pulse flip angle should allow us to determine the quadrupole coupling ω_Q and the heteroatom distances via the value of ϕ in a single crystal, or the quadrupole coupling constant $e^2qQ/\hbar$, the symmetry parameter η and the heteroatom distances in a powdered sample.

[1]H. Ernst, D. Freude, and I. Wolf, Chem. Phys. Lett. **212**, 588 (1993).
[2]K. D. Schmitt, J. Haase, and E. Oldfield, Zeolites **14**, 89 (1994).
[3]E. Oldfield, J. Haase, K. D. Schmitt, and S. E. Schramm, Zeolites **14**, 101 (1994).
[4]Y. Wu, B. Q. Sun, A. Pines, A. Samoson, and E. Lippmaa, J. Magn. Reson. **89**, 297 (1990).
[5]P. J. Grandinetti, J. H. Baltisberger, A. Llor, Y. K. Lee, U. Werner, M. A. Eastman, and A. Pines, J. Magn. Reson. A **103**, 72 (1993).
[6]E. Lippmaa, A. Samoson, and M. Mägi, J. Am. Chem. Soc. **108**, 1730 (1986).
[7]J. Skibsted, E. H. Henderson, and H. J. Jakobsen, Inorg. Chem. **32**, 1013 (1993).
[8]J. Skibsted, N. C. Nielsen, H. Bildsøe, and H. J. Jakobsen, J. Magn. Reson. **95**, 88 (1991).
[9]W. P. Power, Magn. Reson. Chem. **33**, 220 (1995).
[10]D. Massiot, C. Bessada, J. P. Couture, and F. Taulelle, J. Magn. Reson. **90**, 231 (1990).
[11]P. P. Man, J. Klinowski, A. Trokiner, H. Zanni, and P. Papon, Chem. Phys. Lett. **151**, 143 (1988).
[12]P. J. Barrie, Chem. Phys. Lett. **208**, 486 (1993).
[13]K. T. Mueller, J. Magn. Reson. A **113**, 81 (1995).
[14]C. A. Fyfe, K. T. Mueller, H. Grondey, and K. C. Wong-Moon, J. Phys. Chem. **97**, 13 484 (1993).
[15]J.-Ph. Ansermet, C. P. Slichter, and J. H. Sinfelt, Prog. NMR Spectrosc. **22**, 40 (1990).
[16]E. L. Hahn, Phys. Rev. **80**, 580 (1950).
[17]E. Oldfield, C. Coretsopoulos, S. Yang, L. Reven, H. C. Lee, J. Shore, O. H. Han, E. Ramli, and D. Hinks, Phys. Rev. B **40**, 6832 (1989).
[18]A. C. Kunwar, G. L. Turner, and E. Oldfield, J. Magn. Reson. **69**, 124 (1986).
[19]P. P. Man, Solid-State NMR **1**, 149 (1992).
[20]I. Solomon, Phys. Rev. **110**, 61 (1958).
[21]P. P. Man, J. Chim. Phys. **89**, 335 (1992); J. Magn. Reson. **100**, 157 (1992).
[22]M. A. Hepp, P. P. Man, A. Trokiner, and J. Fraissard, Magn. Reson. Chem. **32**, 24 (1994).
[23]P. P. Man, J. Magn. Reson. A **113**, 40 (1995).
[24]P. P. Man, Appl. Magn. Reson. **4**, 65 (1993).
[25]P. P. Man and P. Tougne, Mol. Phys. **83**, 997 (1994).
[26]P. P. Man, Mol. Phys. **78**, 307 (1993); Solid-State NMR **2**, 165 (1993).
[27]A. Wokaun and R. R. Ernst, J. Chem. Phys. **67**, 1752 (1977).
[28]R. R. Ernst, G. Bodenhausen, and A. Wokaun, *Principles of Nuclear Magnetic Resonance in One and Two Dimensions,* International Series of Monographs on Chemistry, Vol. 14 (Clarendon, Oxford, 1990).
[29]A. Abragam, *The Principles of Nuclear Magnetism* (Clarendon, Oxford, 1961).
[30]M. W. Dowley, Solid State Commun. **3**, 351 (1965).
[31]J. Butterworth, Proc. Phys. Soc. London **86**, 297 (1965).
[32]I. D. Weisman and L. H. Bennett, Phys. Rev. **181**, 1341 (1969).
[33]M. Mehring and O. Kanert, Z. Naturforsch. **24a**, 768 (1969).
[34]O. Kanert and M. Mehring, in *NMR Basic Principles and Progress,* edited by P. Diehl, E. Fluck, and R. Kosfeld (Springer-Verlag, Berlin, 1971), Vol. 3.
[35]G. N. Abelyashev, V. N. Berzhanskii, N. A. Sergeev, and Yu V. Fedotov, Sov. Phys. JETP **67**, 127 (1988).
[36]J. Haase and E. Oldfield, J. Magn. Reson. A **101**, 30 (1993); **104**, 1 (1993).
[37]P. P. Man, Chem. Phys. Lett. **168**, 227 (1990).